Sost deficiency leads to reduced mechanical strains at the tibia midshaft in strain-matched *in vivo* loading experiments in mice

Laia Albiol[1,2], Myriam Cilla[3,4], David Pflanz[1], Ina Kramer[5], Michaela Kneissel[5], Georg N. Duda[1,2], Bettina M. Willie[1,6] and Sara Checa[1]

[1]Julius Wolff Institute, Charité-Universitätsmedizin Berlin, Berlin, Germany
[2]Brandenburg School for Regenerative Therapies, Berlin, Germany
[3]Centro Universitario de la Defensa, Academia General Militar, Zaragoza, Spain
[4]Aragon Institute of Engineering Research (I3A), University of Zaragoza, Zaragoza, Spain
[5]Novartis Institutes for BioMedical Research, Basel, Switzerland
[6]Research Centre, Shriners Hospital for Children-Canada, Department of Pediatric Surgery, McGill University, Montreal, Canada

LA, 0000-0002-7409-3858; MC, 0000-0002-8503-9291; GND, 0000-0001-7605-3908; BMW, 0000-0003-2907-3580

Sclerostin, a product of the *Sost* gene, is a Wnt-inhibitor and thus negatively regulates bone accrual. Canonical Wnt/β-catenin signalling is also known to be activated in mechanotransduction. Sclerostin neutralizing antibodies are being tested in ongoing clinical trials to target osteoporosis and osteogenesis imperfecta but their interaction with mechanical stimuli on bone formation remains unclear. *Sost* knockout (KO) mice were examined to gain insight into how long-term *Sost* deficiency alters the local mechanical environment within the bone. This knowledge is crucial as the strain environment regulates bone adaptation. We characterized the bone geometry at the tibial midshaft of young and adult *Sost* KO and age-matched littermate control (LC) mice using microcomputed tomography imaging. The cortical area and the minimal and maximal moment of inertia were higher in *Sost* KO than in LC mice, whereas no difference was detected in either the anterior–posterior or medio-lateral bone curvature. Differences observed between age-matched genotypes were greater in adult mice. We analysed the local mechanical environment in the bone using finite-element models (FEMs), which showed that strains in the tibiae of *Sost* KO mice are lower than in age-matched LC mice at the diaphyseal midshaft, a region commonly used to assess cortical bone formation and resorption. Our FEMs also suggested that tissue mineral density is only a minor contributor to the strain distribution in tibial cortical bone from *Sost* KO mice compared to bone geometry. Furthermore, they indicated that although strain gauging experiments matched strains at the gauge site, strains along the tibial length were not comparable between age-matched *Sost* KO and LC mice or between young and adult animals within the same genotype.

Subject Category:
Life Sciences–Engineering interface

Subject Areas:
biomechanics

Keywords:
Sost, sclerostin, maturation, mechanical strain, finite-element analysis

Author for correspondence:
Sara Checa
e-mail: sara.checa@charite.de

1. Introduction

Sclerostin, a product of the *Sost* gene, negatively regulates bone accrual through Wnt inhibition [1–4]. A deficiency in sclerostin leads to a high bone mass phenotype that is associated with increased bone strength in humans and mice [1]. Mutations of the *Sost* gene and a non-coding deletion 35 kb downstream of this gene leads, respectively, to sclerosteosis and van Buchem's disease in humans [5,6]. Both conditions have similar phenotypes characterized by osteosclerosis and hyperostosis. Apart from syndactyly and minor digital deformities, prenatal skeletal development is normal in humans with sclerosteosis. Postnatal

development is marked by increased longitudinal growth, although closure of the growth plates occurs normally [7]. Also an increased bone mineral density (BMD) with increasing age has been reported in sclerosteosis patients, starting from early childhood [7–9]. Studies on bone material properties performed by Lierop and colleagues [7] revealed lower mineralization and higher heterogeneity of mineralization in young and adult sclerosteosis patients. Also the mineral maturity to crystallinity ratio was lower in these patients compared to healthy controls. These findings are likely to be explained, at least in part, by the higher bone formation observed in sclerosteosis patients, since newer tissue has a lower mineralization.

The *Sost* knockout (KO) mouse model also presents a high bone mass phenotype [10,11], although limited characterization of the bone composition [12,13] and morphology [10,14] has been published. Two studies found the mineral-to-matrix ratio of newly formed cortical and trabecular bone to be significantly lower in *Sost* KO mice than in age-matched wild-type (WT) mice [12,13], while no differences in global bone mineralization were found between the *Sost* KO and WT mice when looking at the whole bone cross section and not just at the newly formed tissue [13]. Contrarily, Li *et al.* and Kramer *et al.* have shown significant higher tissue mineral density (TMD) in trabecular bone of *Sost* KO mice compared to WT [10,11].

As most studies have concentrated on young mice, little is known as to how *Sost* deficiency alters whole bone geometry and TMD after skeletal maturation. Whole bone geometry and TMD affect the local strain environment within the bone, and thus regulate bone adaptation processes [15,16]. Main *et al.* [17] showed that the bones of 26 week old C57Bl/6 mice are more curved than those of 10 week old C57Bl/6 mice, which increases their bending stresses under axial compression loading. The increase in the curvature counteracts effects that age-related increases in mineral and geometric properties of the cross-section have on the bending stresses. No clinical or preclinical studies have yet examined how changes in bone mass or whole bone morphology due to *Sost* deficiency affect the local mechanical strain environment within the bone. This knowledge is particularly relevant since the local strain environment regulates the anabolic response to loading.

Since the anabolic response to loading did not occur with high *Sost* levels [18], it appears that lower levels of *Sost* are essential for the anabolic response to loading to occur. We recently showed an increased bone formation surface (MS/BS) after *in vivo* mechanical loading in 10 week and 26 week old *Sost* KO mice compared to age-matched littermate control (LC) mice [19]. We also observed a greater load-induced (inter-limb difference) total bone gain (Ct.Ar/T.Ar, Ct.Th) in both young and adult *Sost* KO mice compared to LC mice, the inter-limb difference being the difference between the loaded and non-loaded limb of the same animal. Histomorphometric parameters revealed that this gain was achieved through a higher load-induced bone formation at both the periosteal and endocortical surface in the adult *Sost* KO, whereas just the periosteal surface showed a higher load-induced response to loading in young *Sost* KO compared to young LC mice. In contrast, Robling *et al.* [20], showed that load-induced ulnar periosteal bone formation occurred normally in *Sost* KO mice. Morse *et al.* [14] observed a greater response to loading in 10 week old *Sost* KO mice compared to WT at the metaphyseal region (Ct.Th: +23% in *Sost* KO, +8% in WT), but a similar response at the diaphyseal region located at 37% of the total tibial length (Ct.Th: +15% in *Sost* KO, +15% in WT). We recently showed in WT mice that the tibial metaphyseal and mid-diaphyseal regions have a different strain-threshold above which an anabolic response to loading in cortical bone occurs [21], which may explain the region-specific differences. At the 50% mid-diaphyseal region, the same region reported in our study, Morse *et al.* observed a slightly lower response to loading in *Sost* KO compared to WT mice (Ct.Th: 11% in *Sost* KO, 14% in WT).

It is known that the bone anabolic response to loading is diminished in adult compared to young individuals, both in humans and mice [1,22]. Our data show that there is also a reduction of bone mechanoresponsiveness in *Sost* KO mice occurring with maturation [19]. Clinical trials are currently underway to examine the effect of monoclonal antibodies inhibiting sclerostin on bone mass of individuals with osteoporosis [23,24], an age-associated disease, and osteogenesis imperfecta [25], a lifelong disease associated with low bone mass and compromised bone quality. As we are interested in the potential additive effect of loading and sclerostin antibodies on bone gain during growth and skeletal maturation, it is important that we understand how the strain environment changes with skeletal maturation under long-term *Sost* deficiency. Therefore, the aim of this study is to investigate how long-term *Sost* deficiency alters whole bone geometry and TMD and subsequently affects the local strain environment within the bone, since this regulates bone adaptation. Furthermore, we aim to comprehend how the strain environment changes with skeletal maturation under long-term *Sost* deficiency. We hypothesized that strains will be lower in *Sost* KO than in LC mice in regions different from the strain gauge site despite being identical in that particular position (anterior–medial surface of the cortical mid-diaphysis). We tested this hypothesis by investigating the local strain distribution in the bone by *in vivo* strain gauge experiments and finite-element models (FEMs) of young and adult female *Sost* KO and LC mice. These data are critical to our understanding of how long-term *Sost* deficiency is affected by skeletal maturation and whether mechanical loading could enhance bone mass concurrently with sclerostin-neutralizing antibody treatment.

2. Material and methods

2.1. Animals and strain gauging experiments

In this study, mouse tibiae were used to investigate alterations in the bone mechanical behaviour due to *Sost* deficiency and maturation. These mouse tibiae were obtained from 10 and 26 week old *Sost* KO and LC mice ($n = 5$ for 10 week old LC, $n = 7$ for 26 week old LC and 10 week and 26 week old *Sost* KO), which had been used in a previous strain gauging experiment [19]. The limbs were excised after *in vivo*, experimental strain measurement and euthanization.

2.2. *Ex vivo* microCT

Ex vivo microCT imaging of the *Sost* KO and LC bone tibiae was performed. For scan acquisition (Skyscan 1172, Bruker, Kontich, Belgium), the following settings were used: isotropic voxel resolution of 9.91 μm, 100 kVp, 100 μA, 360°, using 0.3° rotation steps and 3 frames averaging. We segmented background and soft tissue voxels from bone voxels by applying a global threshold of 0.650 g cm^{-3} in both ages and genotypes. This threshold, which kept both cancellous and cortical bone voxels, was calculated using the linear attenuation coefficient (μ) distribution of the whole tibia and calculating the minimum between the bone

and the soft tissue peaks. Two phantoms with densities of 0.25 and 0.75 g HA cm^{-3} were used to calculate the tissue mineral density (TMD) based on the μ of the scans. Frequency plots of the microCT images after densitometric calibration can be found in the electronic supplementary material, data S2.

2.3. Bone curvature and morphometric parameters of the cortical bone

We analysed bone curvature and bone morphometric parameters using microCT images ($n = 5$, for 10 week old LC; $n = 7$, 26 week old LC and 10 week and 26 week old *Sost* KO). The binarized scans were manually aligned using commercial software (DataViewer, Bruker, Kontich, Belgium). The minimal and maximal moments of inertia (I_{min}, I_{max}) were calculated for each microCT slice located in the tibial midshaft (5% of the total tibial length centred at 50% of the total tibial length) and averaged. Also the cortical area (Ct.Ar) was determined and averaged in this region. All parameters were calculated using open-source image processing software (BoneJ, ImageJ, NIH, Bethesda, USA) [26]. Since small rotations of the bone cross-section can have a considerable effect on Ct.Ar and moments of inertia, we used not just a three-dimensional view of the bone when aligning it but also projections engendered when cutting it in several planes. After bone realignment, slices at the metaphysis, the tibial central section, the distal tibiofibular junction and the ankle were checked. If one bone was not well aligned, we realigned it again.

We characterized the bone curvature at the central section (CS) of the midshaft by calculating the distance of the centroid of each section to a reference line passing through the centroid of the widest cross-section at the ankle (malleoli) and the centroid of a proximal cross-section located at 10% of the total tibial length (TL) from the tibial condyles (figure 2*a*). This distance was calculated in anterior–posterior (C_{AP}) and in medio-lateral (C_{ML}) directions. The fibula was manually removed from the images before the centroids were calculated. We also measured the TL from the microCT images.

After determining with a Shapiro–Wilks test that the data had a normal distribution, we performed parametric statistics. The between-subject effects of genotype (*Sost* KO mice and LCs) and age (10 week old, 26 week old) as well as their interactions were assessed using a two-way ANOVA (SAS 9.3, Cary, USA). Sub-analyses were performed using independent Student's *t*-test for some datasets. A *p*-value ≤ 0.05 was considered significant.

The per cent difference between genotypes is presented as (*Sost* KO − LC)/LC) × 100%. Age related differences for each of the genotypes are calculated as (26 weeks − 10 weeks)/10 weeks) × 100%.

2.4. Finite-element modelling

FEMs of 10 and 26 week old *Sost* KO and LC tibiae ($n = 1$/age/genotype) were built based on the *ex vivo* microCT data of strain gauged mice tibiae described in §2.2. After image segmentation, a triangular approximation of the bone surface was calculated using an unconstrained smoothing algorithm. The generated surface contained a large number of triangular faces (approx. 7×10^6). To maintain fidelity, the number of faces was progressively reduced with further implementation of best isotropic vertex placement until a 'feasible' triangle number of approximately 0.25×10^6 was achieved. The volume enclosed by the bone surface was then filled with linear four node tetrahedral mesh elements. Thus, we created models with adaptive multi-resolution grids, in which the geometry of the trabecular bone was preserved. All these procedures were performed using commercial software (Amira 5.4.3, FEI, Hillsboro, USA).

2.4.1. Loads and boundary conditions

Loading and boundary conditions aimed to replicate previously reported strain-gauge *in vivo* loading experiments in mouse tibia [19]. A compression load was introduced through the knee with an inclination relative to the bone axis of 10° [27]. The load was applied on a reference node, which was kinematically coupled to the nodes on the surface of the proximal tibial plateau (relative displacements were constrained, relative rotations were kept free). The reference node was allowed to move exclusively in the direction of the applied load. Surface nodes on the distal part of the bone were allowed to move in the anterior–posterior direction but not in the medial–lateral (malleoli constrain this movement) and to rotate around the medial–lateral axis of the tibia, which is the axis of the articulatio talocruralis (hinge joint).

Two different load cases were investigated:

(1) *Load-matched* load case: an identical compression load of −11 N was applied to all groups.
(2) *Strain-matched* load case: a compression load that induced 900 microstrains (με) at the anteromedial aspect of the tibia midshaft, as we have previously measured using *in vivo* strain gauging [19] was applied. Pflanz *et al*. [19] determined that compression loads of −7, −7, −12.9 and −14.5 N induce 900 με at the strain gauge (SG) site in 10 week LC, 26 week LC, 10 week *Sost* KO and 26 week *Sost* KO mice, respectively. The applied axial loads were not scaled for mouse body weight since the aim was to 'replicate' the *in vivo* experiment. These load levels triggered an osteogenic response in all four groups [19]. For this load case, we studied the effect of variations of ±10° in the load axis due to potential misalignments (see electronic supplementary material, data S3).

Boundary conditions and the load were introduced using the same commercial software that we used for the analysis and post-processing (Abaqus 6.12.2, Dassault Systemés Simulia, Providence, USA).

2.4.2. Material properties

Bone material properties were considered linear elastic and isotropic. The Poisson's ratio was set to 0.35 [28] for all models. Heterogeneous models were created in which Young's modulus (E) assigned to each element was estimated using a power-law relationship between the linear attenuation coefficient (μ) and stiffness [28,29]. For a thorough description of the bone material properties assignation, we refer to the electronic supplementary material, data S4. The code for the assignation of μ to the tetrahedral elements and the code for the final model-assembly are included as electronic supplementary material, data S6.

In addition, to isolate the influence of bone geometry on the predicted strains, we developed homogeneous models with an identical Young's modulus of 12 GPa for all elements in all groups. In 10 and 26 week old LC and in 10 week old *Sost* KO, the proximal tibio-fibular junction was not completely mineralized. Therefore, a linear elastic material with a Young's modulus of 1.6 MPa and Poisson's ratio of 0.2 was used to model this non-mineralized region, according to values found in the literature for mouse cartilage [30]. This approach has been followed by other groups developing FEMs of the tibia of young C57Bl/6 mice [31].

In the 10 week old LC, we additionally found that the mineralization at the growth plate was so low that there was a disconnection between the epiphysis and metaphysis in the meshed models. We remeshed the model including the growth plate and manually assigned to this region the same material properties that we used for the cartilage of the tibio-fibular junction.

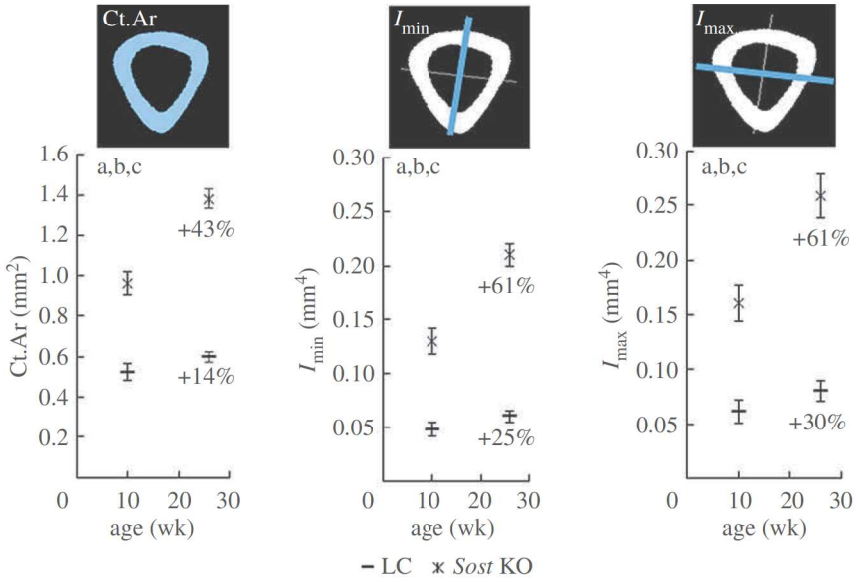

Figure 1. Morphometric parameters of the cortical bone at the tibial midshaft: cortical area (Ct.Ar) and maximal and minimal moments of inertia (I_{max}, I_{min}). *ANOVA. Main effects*: (a) genotype, (b) age; *Interactions*: (c) genotype × age. $p < 0.05$. The percentages indicate the increase of the morphometric parameters with maturation in each genotype.

2.4.3. Data analysis

Heterogeneous FEMs ($n = 1$/age/genotype) were validated by comparing the predicted strains at the strain gauge site (*strain-matched* load case) to the strains measured in the *in vivo* loading experiments previously reported [19]. The strain gauge position was, after removal of the metallic parts, still visible in the microCT scans. From the microCT scans, we measured that the strain gauges had been positioned, on average, at 41% of the whole tibial length measured from the proximal end. The corresponding predicted strain gauge value for each bone was calculated by averaging the strain in the direction of the strain gauge at its mounting position (ε_{xx}).

We calculated the structural stiffness of the bone in all groups by dividing the load in the bone axis direction by the displacement of the reference node in this same direction.

For each element within the heterogeneous and homogeneous FEMs, the maximum absolute value between the maximal (tensile, ε_{max}) and minimal (compressive, ε_{min}) principal strains was calculated. Thereafter, the mean values of the tensile ($\bar{\varepsilon}_{max}$) and compressive ($\bar{\varepsilon}_{min}$) strains in each cross-section along the bone length were determined. Elements for which $abs(\varepsilon_{max}) > abs(\varepsilon_{min})$ were used to calculate $\bar{\varepsilon}_{max}$ and s.d.(ε_{Max}), elements for which $abs(\varepsilon_{Max}) \leq abs(\varepsilon_{Min})$ were used to calculate $\bar{\varepsilon}_{min}$ and s.d.(ε_{min}), where s.d. stands for standard deviation. We focused on the CS of the midshaft since it is the centre of the region of interest (ROI) in which bone formation and resorption in response to loading has been previously evaluated in this mouse model [19].

3. Results

3.1. Bone morphology

The ANOVAs performed on the morphological parameters of the cortical bone showed that both genotype and age have a significant effect on the Ct.Ar, I_{min} and I_{max} (figure 1) at the tibial midshaft. The *t*-tests revealed significant genotype related differences in Ct.Ar, I_{min} and I_{max} for both the 10 week and the 26 week old animals. Ct.Ar, I_{min} and I_{max} were 84%, 171% and 161% higher in the 10 week *Sost* KO than in the 10 week old LC. The genotype related differences were even more dramatic in the adult animals with 131% higher Ct.Ar, 249% higher I_{min} and 223% higher I_{max} in 26 week *Sost* KO compared with the age-matched LC ($p < 0.0001$ for all three variables and both ages). Skeletal maturation led to a significantly greater Ct.Ar, I_{min} and I_{max} in the tibial midshaft of the *Sost* KO and LC mice (figure 1).

Regarding bone curvature, the ANOVA showed no significant difference either in the C_{ML} or the C_{AP} at the midshaft between *Sost* KO and their age-matched LCs (figure 2). In contrast, animal age was found to have a significant effect on the C_{AP} and C_{ML}. The *t*-tests revealed that adult LC mice had significantly greater C_{AP} (+142%) and C_{ML} (+32%) than young LC mice, but this age-related effect on whole bone curvature was not measured in the *Sost* KO mice (table 1).

As expected, the tibiae of both *Sost* KO and LC mice were significantly longer at the age of 26 weeks than at the age of 10 weeks (table 1). Both young and adult *Sost* KO mice showed a significantly greater tibial length than aged-matched LCs (TL = +3.5% for the 10 week old and TL = +2.4% for the 26 week old mice).

3.2. Bone tissue mineral density and bone stiffness

The 10 week old LC mouse showed higher bone volume with low TMD values compared with the 26 week old LC (figure 3*a*). The 10 and 26 week old *Sost* KO mice showed similar TMD distributions, which were between the values obtained for the 10 and 26 week old LC mice. Accordingly, higher amounts of bone volume were characterized by a low Young's modulus in the 10 week old compared to the 26 week old LC heterogeneous model (figure 3*b*,*c*). Age-related differences in the mean distribution of tissue stiffness were not observed between 10 and 26 week *Sost* mice (figure 3*b*), however regional differences were observed. For example, a larger tissue volume presented high stiffness at the midshaft in the 26 week old compared with 10 week old *Sost* mice (figure 3*c*). The mean Young's modulus of the heterogeneous FEMs was similar between 10 and 26 week old *Sost* KO animals (10.67 GPa for the 10 week old *Sost* KO, 10.79 GPa for the 26 week old *Sost* KO). A lower mean Young's modulus was determined for the 10 week old compared with the 26

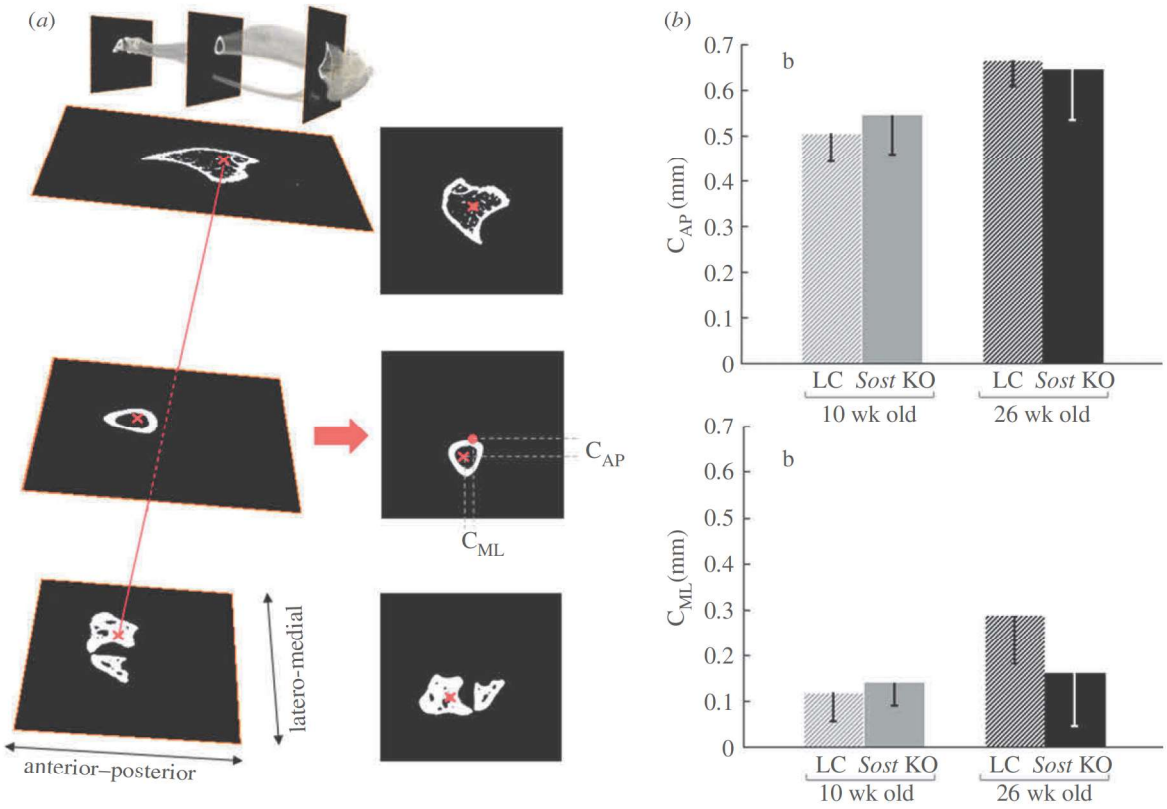

Figure 2. (*a*) Graphical description of the method used to quantify bone curvature from microCT images. (*b*) Bone curvature in mediolateral (C_{ML}) and antero-posterior directions (C_{AP}). *ANOVA. Main effects*: (a) genotype, (b) age; *Interactions*: (c) genotype × age. $p < 0.05$.

Table 1. Mean ± s.d. of all parameters used to describe bone morphology at the cortical midshaft. + indicates age related differences and * significant differences between genotypes.

	10 week old		26 week old	
	LC	*Sost* KO	LC	*Sost* KO
Ct.Ar (mm^2)	0.520 ± 0.040	0.963 ± 0.057*	0.599 ± 0.027$^+$	1.380 ± 0.047*$^+$
I_{min} (mm^4)	0.048 ± 0.006	0.130 ± 0.012*	0.060 ± 0.005$^+$	0.210 ± 0.010*$^+$
I_{max} (mm^4)	0.062 ± 0.011	0.161 ± 0.017*	0.080 ± 0.009$^+$	0.259 ± 0.020*$^+$
C_{ML} (mm)	0.12 ± 0.06	0.14 ± 0.05	0.29 ± 0.10$^+$	0.16 ± 0.12
C_{AP} (mm)	0.51 ± 0.06	0.55 ± 0.09	0.67 ± 0.06$^+$	0.65 ± 0.11
TL (mm)	16.47 ± 0.15	17.05 ± 0.14*	17.23 ± 0.07$^+$	17.65 ± 0.12*$^+$

*$p < 0.05$ compared to age-matched LC.
$^+p < 0.05$ compared to young mice with same genotype.

week LC mouse (9.87 GPa for the 10 week old LC, and 11.16 GPa for the 26 week old LC).

3.3. Mechanical strains within the tibiae of *load-matched Sost* knockout and littermate control mice

When comparing the age-matched genotypes using homogeneous FEMs under the same compression load, the diminished strains, due to increased bone mass in *Sost* deficient mice becomes visible (figure 4*a*). Tensile strains were on average 52% lower in the 10 week old *Sost* KO than in the age-matched LC, whereas they were 63% lower (in absolute value) for the adult *Sost* KO than for the adult LC (figure 4*b*). The compressive strains were on average 50% lower in the 10 week old *Sost* KO than in the age-matched LC, whereas they were 62% lower for the adult *Sost* KO than for the adult LC. Interestingly, these differences were more pronounced in the diaphyseal midshaft than in the rest of the bone for both tension and compression. Maturation led to lower strains in both the LC and the *Sost* KO mice, with the decrease being much more pronounced in the *Sost* KO than in the LC.

Heterogeneous FEMs, to compare the age-matched genotypes under the same compression load, led to similar strain distribution within the tibia when compared to the strains obtained with the homogeneous models (electronic supplementary material, data S5).

3.4. Mechanical strains within the tibiae of *strain-matched* Sost knockout and littermate control mice

The predicted strains at the strain gauge site by heterogeneous FEMs were: 1085 με young *Sost* KO, 1010 με young LC, 870 με

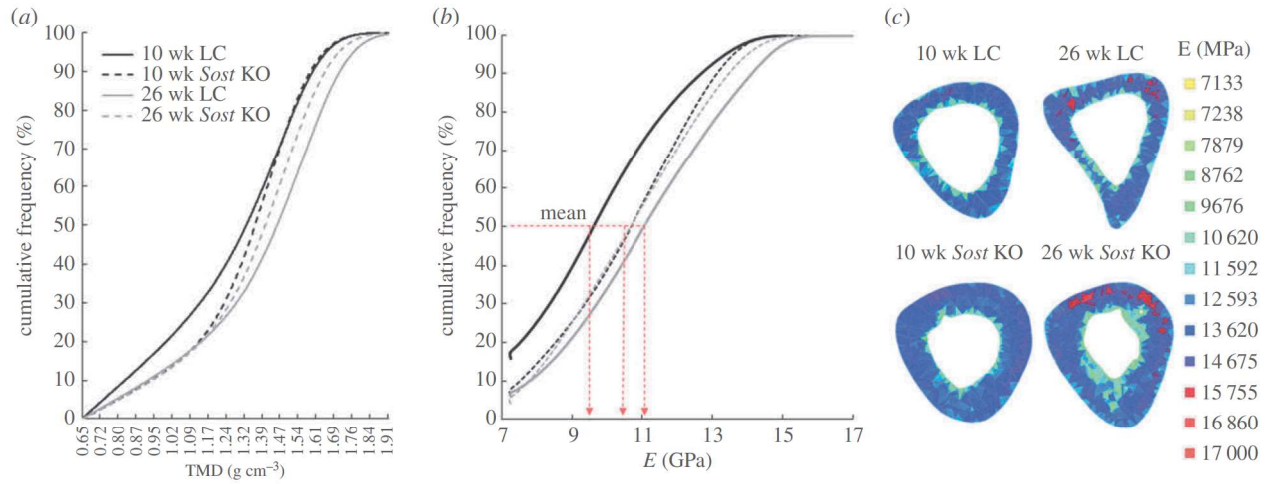

Figure 3. (*a*) TMD cumulative frequency for the bony voxels of the segmented scans. (*b*) *E* cumulative frequency for the bony elements of the FEMs. (*c*) *E* distribution within the central section of the midshaft for all four FEMs.

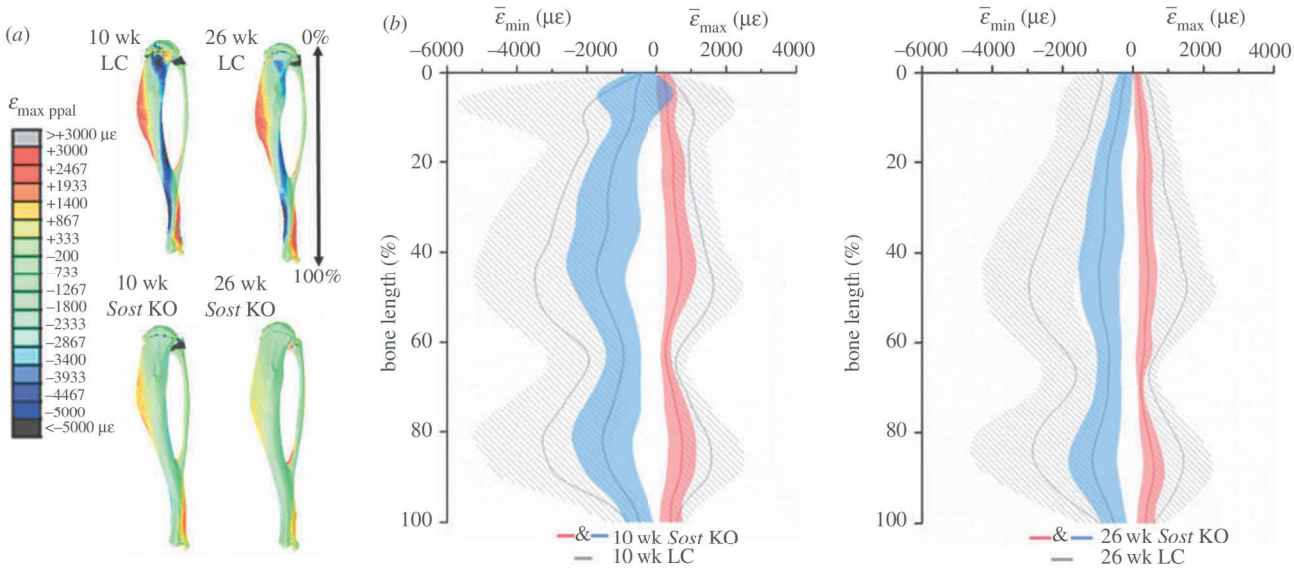

Figure 4. Maximal principal strain ($\varepsilon_{max\ ppal} = \max(|\varepsilon_{min}|, |\varepsilon_{max}|)$ distribution (*a*) and mean tensile and compressive strains (*b*) along the length of the tibia. Homogeneous models with identical material properties ($E = 12$ GPa) under an 11 N compressive load (*load-matched* load case). Lines represent $\bar{\varepsilon}_{max}$ and $\bar{\varepsilon}_{min}$. Shaded regions correspond to $\pm$s.d. (ε_{max}) and $\pm$s.d. (ε_{min}), where s.d. stands for standard deviation, which reflects the range of ε_{max} for tension and ε_{min} for compression within the cross-section.

adult *Sost* KO and 862 με adult LC. The whole-bone stiffness was: 290 N mm^{-1} in the young *Sost* KO, 122 N mm^{-1} in the young LC, 409 N mm^{-1} in the adult *Sost* KO and 165 N mm^{-1} in the adult LC.

When comparing age-matched mice using heterogeneous FEMs, mean tensile and compressive predicted strains in cortical bone were higher for LC than for *Sost* KO mice along the whole tibia (figure 5) except for its distal end, where the strains were slightly higher in the *Sost* KO.

At the tibial midshaft region (47.5% to 52.5% of tibial length), large differences between genotypes in both ages were found, with higher strains in LC mice compared with the age-matched *Sost* KO (table 2). Establishing a comparison between ages, adult animals showed lower strains than young mice with the same genotype for both tension (28% for the *Sost* KO and 5% for the LC) and compression (31% for the *Sost* KO and 16% for the LC).

Although predicted strains at the strain gauge site were similar between aged-matched genotypes, maximum tensile strains at the central section of the tibial midshaft were considerably higher in the LC compared to *Sost* KO mice, in both age groups (figure 6).

4. Discussion

In this study, we investigated the long-term effects of sclerostin deficiency in bone morphology, material properties and the mechanical environment within the tibia in young and adult mice. We found that long-term sclerostin deficiency leads to changes in bone morphology, which result in decreased mechanical strains within the cortical bone. The decreased strains can be observed even at the mid-shaft region, where we previously reported an increased response to mechanical loading in female *Sost* KO mice [19]. In agreement with Morse *et al.* [14], we showed the tibiae of the *Sost* KO to have a notably greater cortical area and moment of inertia than those from the LC mice.

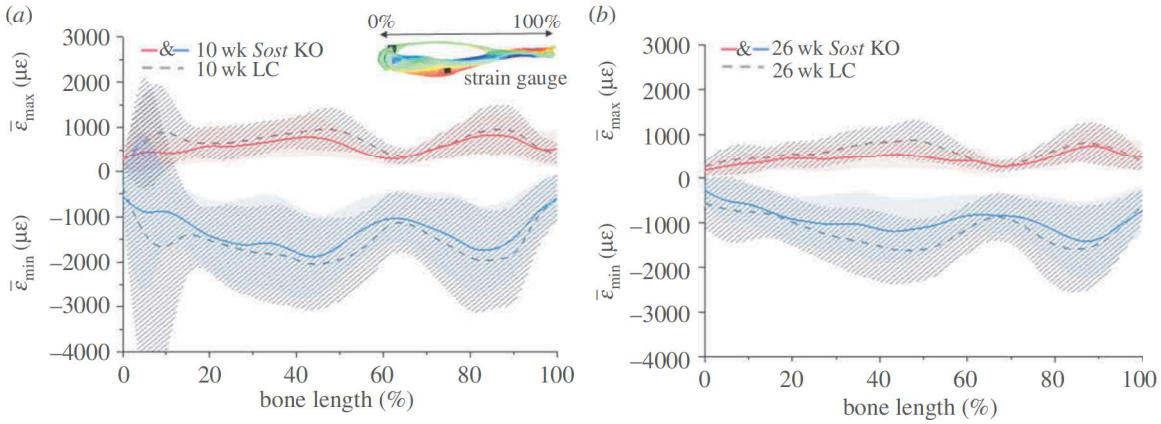

Figure 5. Mean tensile and compressive strains along the length of the tibia for the heterogeneous FEMs of the 10 (*a*) and 26 (*b*) week old female *Sost* KO and LC mice. *Strain-matched* load case. Lines represent $\bar{\varepsilon}_{max}$ and $\bar{\varepsilon}_{min}$. Shaded regions correspond to $\pm$s.d. (ε_{max}) and $\pm$s.d. (ε_{min}), where s.d. stands for standard deviation, which reflects the range of ε_{max} for tension and ε_{min} for compression within the cross-section.

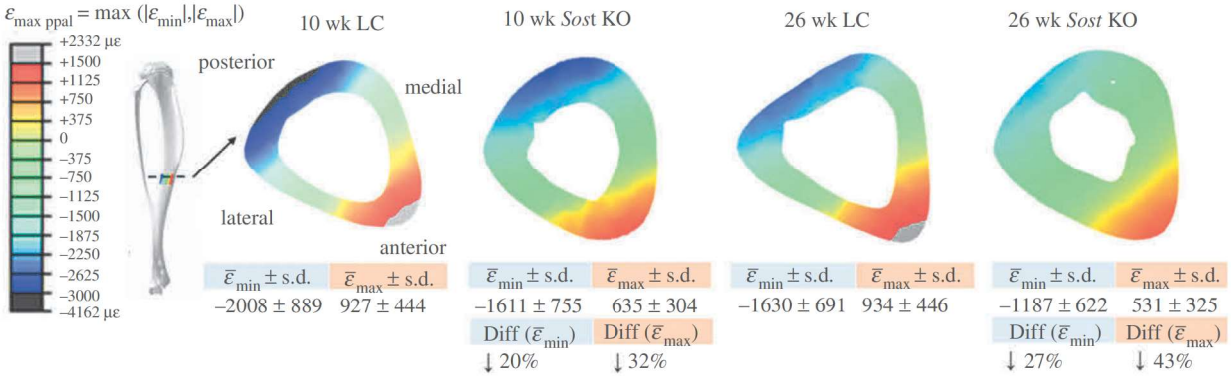

Figure 6. Strain distribution in the cross section located in the middle of the tibia. Heterogeneous models, *strain-matched* load case. Percentages indicate the strain difference between *Sost* KO and their age matched LC (*Sost* KO − LC)/LC) × 100%.

Table 2. Mean compressive ($\bar{\varepsilon}_{min}$) and tensile strains ($\bar{\varepsilon}_{max}$) at the tibial midshaft region (47.5% to 52.5% of tibial length). *Strain-matched* load case.

	10 week old		26 week old	
	LC	*Sost* KO	LC	*Sost* KO
$\bar{\varepsilon}_{min}$ (με)	−1968 ± 893	−1653 ± 752	−1663 ± 668	−1140 ± 611
$\bar{\varepsilon}_{max}$ (με)	921 ± 460	706 ± 381	874 ± 460	505 ± 285

Although we recognize that the assessment of volumetric TMD using polychromatic microCT has limitations [32], we aimed to consider the effects of regional differences in TMD on the strain environment. Two studies [10,11] report significantly increased TMD in the trabecular bone of the distal metaphysis of the femora of 17 week old female *Sost* KO compared with WT. Contrarily, Ross and colleagues [13] found no significant differences on the global bone mineralization, measured with bSEM, between the *Sost* KO and the WT mice. Similar to this finding [13] but not to other data [10,11], we did not observe dramatic differences between the TMD distribution in the adult *Sost* KO and the aged-matched LC mice. It should be mentioned that even though the TMD was assessed locally to calculate an estimated Young's modulus, the average values that we report are for the whole bone and no distinction between small compartments of either cortical or trabecular bone have been analysed separately, as the above referenced studies did [10,11].

The differences in the TMD distribution between the young *Sost* KO and LC mice were more pronounced than between adult mice, but we think that they rather rely on the phenotypic singularities and the apparently delayed maturation that we found in the LC. We found that the LC mice had a larger growth plate (non-mineralized tissue) in the proximal tibia compared to what we have observed previously in C57Bl/6 mice [28]. Since canonical Wnt signalling promotes maturation of chondrocytes, which express sclerostin themselves when terminally differentiated, it has been speculated that lack of sclerostin may favour increased differentiation towards hypertrophic chondrocytes which results in a larger hypertrophic zone in the growth plate [23]. We cannot explain the reasons for the abnormal growth plate in the LC mice but they could be related to an insufficient production of sclerostin by heterozygote mothers, which has influence on the endochondral ossification of their homozygote +/+ offspring. A genetic drift is extremely

unlikely since breeding programmes at animal facilities are designed to avoid them.

Bone curvature was considerably higher in the anterior–posterior direction (C_{AP}) compared to the medial–lateral direction (C_{ML}) in both LC and *Sost* KO mice. This finding has also been previously shown in young growing (6 to 16 week old) female C57Bl/6 mice [17]. C_{AP} plays a key role in the amount of bending engendered by a compressive load and thus it is one of the major contributors to the tensile strains at the anterior part of the tibia. No significant difference either in anterior–posterior or medial–lateral direction were found at the midshaft between *Sost* KO and their age-matched LCs.

We used both homogeneous and heterogeneous FEMs to characterize the mechanical environment within the bone due to controlled external loading. Homogeneous models allowed us to isolate the influence of bone geometry on the induced strains, while heterogeneous models gave us insight into how the TMD was influencing the strains. When introducing an identical compressive load to all four models (*load-matched* experiment) the strains in the tibiae of the *Sost* deficient were dramatically lower than in their age-matched LC for both the heterogeneous and homogeneous models. Interestingly, these differences in the strains were more pronounced at the diaphyseal midshaft than the rest of the bone in both tension and compression. The region of the midshaft is commonly used to characterize cortical bone, so further studies assessing bone formation in *Sos*t KO mice and using littermate mice as controls should consider this fact. Also the most distal part of the bone (80–90% bone-length) was a region of pronounced differences between the *Sost* KO animals and their age-matched LC.

Previous studies examining the anabolic response to mechanical loading in *Sost* KO mice did not use LC mice, but rather WT controls. These mice should display more variability in terms of basal Sost expression, due to differing genetic backgrounds. In the present study, we ensured the animals were from the same breeding pair to avoid such variability. The use of LC is even more important considering the growth plate anomaly we observed in *Sost*+/+ mice. Additionally, none of the studies so far published included FEMs to examine the strain distribution during *in vivo* loading, but only relied on strain gauging at a single site on the tibia [14] or on extrapolations based on the ulnar strains of a different mice strain [20]. This work shows that strain gauge-based *strain-matched* experiments do not ensure comparable strains along the tibiae of *Sost* KO and LC mice and that *in silico* models are needed to assess the strain environment.

The present work reveals that the use of heterogeneous FEMs leads to small differences in the strain distribution within the tibia when compared to the strains obtained with the homogeneous models. The homogeneous models predicted higher strains than the heterogeneous models in the mid-diaphysis for both ages and phenotypes, both in tension and compression, although the Young's modulus (E) used for the homogeneous models (12 GPa) is higher than the average E of the corresponding heterogeneous model (figure 3*b*). This can be explained since the TMD at the mid-diaphysis is higher than in other regions of the bone and so is the E assuming the power law relationship between TMD and E used in this work (figure 3*c*). We conclude that for tissue level models like the ones presented here, homogeneous models provide results that are accurate enough. Nevertheless, the choice of the E should not be made just under consideration of the average E for the whole bone but also considering the local stiffness of the region of interest and its relationship to the average stiffness.

Heterogeneous FEMs predicted similar strain levels to those we measured in strain gauge experiments at the midshaft of *Sost* KO and LC mice for the *strain-matched* load case [19]. The whole bone stiffness of the young *Sost* KO was 137% higher than the whole bone stiffness of the young LC, while the adult *Sost* KO had a 147% higher whole bone stiffness than the adult LC. Yang *et al*. [31] reported that the whole bone stiffness of their heterogeneous FEM of a 16 week old WT mouse was approximately 180 N mm^{-1}, which is in good agreement with the 122 N mm^{-1} for the 10 week LC and the 165 N mm^{-1} for the 26 week old LC presented here. The same strain level at the gauge site did not ensure comparable strains along the whole tibial length in *Sost* KO and LC mice. In both age groups, FEMs predicted lower mechanical strains along the length of the tibiae in *Sost* KO compared to LC mice.

Morse *et al*. [14] reported significant higher increase of BV in the cortical midshaft of 10 week old *Sost* KO mice compared to WT after a *strain-matched* loading regime. The load levels determined by Morse and their colleagues do not match our strain gauge experiments [19]. They applied a compression load of −12.5 N to engender 1200 με in the midshaft of 10 week old *Sost* KO mice, while we determined that −12.9 N engenders 900 με. Discrepancies could be due to strain gauge positioning, since the strain gradients in the strain gauge region are high. Differences between the two studies in the bone anabolic response to loading could also be due to control mice used.

Interestingly, Morse *et al*. [14] report the increase in cortical BV to be the highest around 2.12 mm below the growth plate, which will correspond to the 14% of the total tibial length (TL), while it remains small around the midshaft. They speculate that higher strains in the metaphyseal region could be the origin of the higher increase on cortical BV occurring with loading. Our results (10 week old *Sost* KO, strain-matched load case) contradict this hypothesis since $\bar{\varepsilon}_{Max}$ at 14% of TL and 50% of TL are similar and $\bar{\varepsilon}_{Min}$ is higher (more negative) at the midshaft than at the cortical bone in the metaphysis.

We have previously shown that the cortical adaptive formation response in the midshaft was enhanced in female *Sost* KO compared to LC mice [19]. Loading-induced gains in mineralizing surface were enhanced in *Sost* KO mice, although the FEMs in the current study predict lower mean compressive ($\bar{\varepsilon}_{Min}$) and tensile strains ($\bar{\varepsilon}_{Max}$) in female *Sost* KO compared to LC mice. Our histomorphometric data reveal that bone formation (MS/BS, MAR) is higher in the endosteal surface than in the periosteal, for both *Sost* KO and LC mice. *Sost* KO mice showed an increased bone formation in response to loading (interlimb difference) at both the endosteal and periosteal surface, although the effect is most pronounced at the periosteum surface. A qualitative analysis of the strains in the loaded limb at the tibial midshaft (figure 6) reveals that strains in the periosteum of the *Sost* KO mice are lower than in their age matched LCs for both tension and compression. This is particularly surprising since our previous studies in WT mice have shown an enhanced bone formation response at the endosteal surface compared to the periosteal surface despite increased strains at the periosteal surface [33]. Nevertheless, in the present study we are not able to elucidate if the enhanced anabolic response to loading is because the strains in the endosteum remain under a certain threshold or due to biological, non-mechanically related factors. We cannot conclude that a

lower strain-threshold triggers an osteogenic response in *Sost* KO. For that, a correlation between formation events and the strain environment in the surrounding area, as performed in [21], must be determined.

Our previous study [19] showed that ablation of the *Sost* gene in mice resulted in an increased expression of another Wnt inhibitor, *Dkk1*, possibly due to a feedback mechanism intended to compensate for the loss of *Sost*. Similar to other reports (Holguin *et al*. [22]) *Dkk1* expression was significantly downregulated with loading (loaded versus control non-loaded limb). The enhanced bone formation response to loading observed in *Sost* KO mice compared to LC mice suggest that *Dkk1* was not sufficient to compensate for the loss of *Sost*. In addition to altered Wnt signalling, other mechanosensitive signalling pathways are likely activated in the absence of *Sost*.

It is known that there is a loss of mechanosensation occurring with ageing in both humans and mice [1,22] and it is known as well, that physiologic sclerostin levels increase with age in humans, causing a decrease in Wnt canonical signalling. Thus, clinical trials are underway to determine if sclerostin neutralizing antibodies can maintain Wnt-signalling activation in patients with low bone mass. We also showed that the anabolic response to loading was reduced at maturation in both LC and *Sost* KO mice coincident with age-dependent expression of Wnt target genes in *Sost* KO and LC mice as well as *Sost* gene expression in LC mice [19]. The *strain-matched* load case reveals that both the mean maximal principal strain ($\bar{\varepsilon}_{max}$) and mean minimal principal strain ($\bar{\varepsilon}_{min}$) are lower in the tibial midshaft of the adult mice compared to the young mice, so we cannot exclude that lower tensions are, at least in part, responsible for the reduced anabolic response of the adult mice.

Skeletal maturation led to a significant increase in Ct.Ar, I_{min} and I_{max} in the *Sost* KO animals. In contrast to LC mice, where a significant increase in C_{AP} was observed in adult compared to young mice, the C_{AP} did not increase significantly with maturation in *Sost* KO mice (table 1). With their greater area and moments of inertia and non-increased bone curvature, *Sost* KO mice present all possible geometrical features that lead to low strains in their cortical midshaft. These results likely explain why the strains in the central portion of the adult *Sost* KO tibia FEM are remarkably lower than in the central portion of the young *Sost* KO tibia FEM, although the strains at the strain gauge site are similar. Interestingly, our histomorphometric data revealed that the greater load-induced bone gain observed in both young and adult *Sost* KO mice was achieved through higher bone formation at both the periosteal and endocortical surface in the adult *Sost* KO, whereas just the periosteal surface showed a higher response to loading in young *Sost* KO compared to young LC mice. These findings support the hypothesis that lower strain thresholds trigger an osteogenic response in *Sost* KO even in adult mice, but, as we have already mentioned, a correlation between formation events and the strain environment must be performed to test this hypothesis.

This work has limitations. Variability of the tibial morphologic parameters between specimens within the same age and phenotype was small (figures 1 and 2) therefore one FEM per phenotype and age was created. Razi *et al*. [28] and Yang *et al*. [29] showed that small differences in bone morphology between female C57BL/6 J mice of the same age led to very similar strain distributions. The models predicted very high compressive strains in the cortical bone of the metaphyseal region of the young and adult LC animals. The increased size of the growth plate in the LC, compared to *Sost* KO and age-matched WT female C57BL/6 J [28], will likely lead to an overestimation of the strains predicted by the models in this region, especially in the cartilage–bony element interface. A more accurate modelling of this interface and a mesh with very small elements in this region are required to evaluate with precision the strain environment of the cortical bone of the metaphysis. In this study we did not investigate the mechanical environment in the tibia of elderly *Sost* KO mice. This was motivated by several reasons including the increased mortality observed in elderly *Sost* KO mice in our breeding programme, which would have required an excessive number of animals. Also, the load levels necessary to reach osteogenic mechanical strain levels for corresponding experimental studies in elderly *Sost* KO mice would have damaged the joints and thus were not performed [19].

We investigated the effect of *Sost* deficiency and skeletal maturation on whole bone morphology and the local mechanical strain environment induced within the bone under external controlled *in vivo* loading. Our key findings were: (i) the differences in Ct.Ar, I_{min} and I_{max} between age-matched *Sost* KO compared to LC mice were much more dramatic in the adult mice, suggesting that the phenotypic changes in bone mass observed in *Sost* deficient mice follow an increasing trend until they reach adulthood. This fact is reflected in the mechanical environment within the bone: differences occurring with maturation were higher for the *Sost* KO than for the LC mice. (ii) TMD is a minor contributor to the strain distribution in tibia cortical bone compared to bone geometry in *Sost* KO mice. This finding is in agreement with what has been already shown for C57Bl/6 mice [28,29]. (iii) The strains in the tibiae of the *Sost* deficient mice are dramatically lower than in age-matched LC mice under an externally applied compressive load. These differences are especially pronounced in the diaphyseal midshaft, a region that is commonly used to assess anabolic and catabolic changes on cortical bone. (iv) Matching the strain level at a single point on the bone surface of the tibial mid-diaphysis, where a strain gauge can be placed *in vivo*, does not ensure comparable strains along the entire length of the tibia in age-matched *Sost* KO and LC mice. It also does not ensure comparable strains along the tibial length of young and adult animals within the same genotype, with discrepancies observed to be greater for the *Sost* KO than for the LC mice.

It is important that we understand how long-term sclerostin inhibition alters the strains environment in bone and furthermore how bone anabolic and catabolic processes are affected by it. This knowledge is crucial to determine in which grade a multimodal therapy including sclerostin-antibody and mechanical stimuli could have additive or synergistic effects on bone formation. Sclerostin neutralizing antibodies are being tested in ongoing clinical trials to target osteoporosis [23,24], and other low bone mass disorders such as osteogenesis imperfecta [25]. Thus, maturity-dependent differences in bone strains should be considered when conceiving those multimodal therapies. *Sost* KO mice are a widely used model to study the effects of long-term sclerostin inhibition. Data from the current study show decreased strains in both tension and compression at the cortical midshaft of young

and adult *Sost* KO mice compared to age-matched LC even in strain-matched load conditions. Surprisingly, our previous work has shown an increase of load induced bone formation surface relative to total surface (MS/BS) in young and adult *Sost* KO mice compared to age-matched LC in this region. Together these data suggest that even physical activity which engenders low strain magnitudes, in combination with sclerostin inhibition, may be a promising anabolic therapy, although age-dependent mechano-responsiveness must be considered.

Ethics. All animal experiments described were carried out according to the policies and procedures approved by the local legal research animal welfare representative (LaGeSo Berlin, G0021/11).

Data accessibility. In compliance with the EPSRC's open access initiative, the datasets and code for analysis are included in the main text of the manuscript or in the electronic supplementary material, data section (see S1–S6).

Authors' contributions. L.A.: laboratory work, methods development, data analysis and interpretation, article writing. M.C.: methods development, article revising. D.P.: laboratory work, article revising. I.K.: study conception, article revising. M.K.: study conception, article revising. G.N.D.: study conception, article revising. B.M.W.: study conception, data analysis and interpretation, article writing. S.C.: changes in study design, data interpretation, article writing. All authors gave final approval for publication.

Competing interests. The initial four male *Sost* KO mice that underwent embryo transfer were provided by Novartis. Two authors (I.K. and M.K.) are employed by Novartis. No funding was received for this project by Novartis Ltd.

Funding. This study was partially supported by the German Federal Ministry of Education and Research (Bundesministerium für Bildung und Forschung: TP5/DIMEOs), the German Research Foundation (Deutsche Forschungsgemeinschaft; WI-3761/4-1, CH-1123/4-1, DU-298/21-1), Shriners Hospitals for Children, and the Réseau de recherche en santé buccodentaire et osseuse recruitment aid programme.

References

1. Bonewald LF, Johnson ML. 2008 Osteocytes, mechanosensing and Wnt signaling. *Bone* **42**, 606–615. (doi:10.1016/j.bone.2007.12.224)
2. Lin C *et al.* 2009 Sclerostin mediates bone response to mechanical unloading through antagonizing Wnt/β-catenin signaling. *J. Bone Miner. Res.* **24**, 1651–1661. (doi:10.1359/jbmr.090411)
3. Issack PS, Helfet DL, Lane JM. 2008 Role of Wnt signaling in bone remodeling and repair. *HSS J.* **4**, 66–70. (doi:10.1007/s11420-007-9072-1)
4. Kang KS, Robling AG. 2015 New insights into Wnt-Lrp5/6-β-catenin signaling in mechanotransduction. *Front. Endocrinol.* **5**, 455.
5. Balemans W *et al.* 2001 Increased bone density in sclerosteosis is due to the deficiency of a novel secreted protein (SOST). *Hum. Mol. Genet.* **10**, 537–543. (doi:10.1093/hmg/10.5.537)
6. Brunkow ME *et al.* 2001 Bone dysplasia sclerosteosis results from loss of the SOST gene product, a novel cystine knot-containing protein. *Am. J. Hum. Genet.* **68**, 577–589. (doi:10.1086/318811)
7. van Lierop AH, Appelman-Dijkstra NM, Papapoulos SE. 2017 Sclerostin deficiency in humans. *Bone* **96**, 51–62. (doi:10.1016/j.bone.2016.10.010)
8. Gardner JC, van Bezooijen RL, Mervis B, Hamdy NA, Lowik CW, Hamersma H, Beighton P, Papapoulos SE. 2005 Bone mineral density in sclerosteosis; affected individuals and gene carriers. *J. Clin. Endocrinol. Metab.* **90**, 6392–6395. (doi:10.1210/jc.2005-1235)
9. van Lierop AH, Hamdy NA, Hamersma H, van Bezooijen RL, Power J, Loveridge N, Papapoulos SE. 2011 Patients with sclerosteosis and disease carriers: human models of the effect of sclerostin on bone turnover. *J. Bone Miner. Res.* **26**, 2804–2811. (doi:10.1002/jbmr.474)
10. Li X *et al.* 2008 Targeted deletion of the sclerostin gene in mice results in increased bone formation and bone strength. *J. Bone Miner. Res.* **23**, 860–869. (doi:10.1359/jbmr.080216)
11. Kramer I, Loots GG, Studer A, Keller H, Kneissel M. 2010 Parathyroid hormone (PTH)-induced bone gain is blunted in SOST overexpressing and deficient mice. *J. Bone Miner. Res.* **25**, 178–189. (doi:10.1359/jbmr.090730)
12. Hassler N *et al.* 2014 Sclerostin deficiency is linked to altered bone composition. *J. Bone Miner. Res.* **29**, 2144–2151. (doi:10.1002/jbmr.2259)
13. Ross RD, Mashiatulla M, Robling AG, Miller LM, Sumner DR. 2016 Bone matrix composition following PTH treatment is not dependent on sclerostin status. *Calcif. Tissue Int.* **98**, 149–157. (doi:10.1007/s00223-015-0074-6)
14. Morse A, McDonald MM, Kelly NH, Melville KM, Schindeler A, Kramer I, Kneissel M, Van Der Meulen MCH, Little DG. 2014 Mechanical load increases in bone formation via a sclerostin-independent pathway. *J. Bone Miner. Res.* **29**, 2456–2467. (doi:10.1002/jbmr.2278)
15. Rubin CT, Lanyon LE. 1984 Regulation of bone formation by applied dynamic loads. *J. Bone Joint Surg. Am.* **66**, 397–402. (doi:10.2106/00004623-198466030-00012)
16. Duffy MP, Jacobs CR. 2015 Seeing the unseen: cell strain and mechanosensing. *Biophys. J.* **108**, 1583–1584. (doi:10.1016/j.bpj.2015.03.008)
17. Main RP, Lynch ME, van der Meulen MC. 2010 *In vivo* tibial stiffness is maintained by whole bone morphology and cross-sectional geometry in growing female mice. *J. Biomech.* **43**, 2689–2694. (doi:10.1016/j.jbiomech.2010.06.019)
18. Tu X *et al.* 2012 Sost downregulation and local Wnt signaling are required for the osteogenic response to mechanical loading. *Bone* **50**, 209–217. (doi:10.1016/j.bone.2011.10.025)
19. Pflanz D *et al.* 2017 Sost deficiency led to a greater cortical bone formation response to mechanical loading and altered gene expression. *Sci. Rep.* **7**, 9435. (doi:10.1038/s41598-017-09653-9)
20. Robling AG, Kang KS, Bullock WA, Foster WH, Murugesh D, Loots GG, Genetos DC. 2016 Sost, independent of the non-coding enhancer ECR5, is required for bone mechanoadaptation. *Bone* **92**, 180–188. (doi:10.1016/j.bone.2016.09.001)
21. Birkhold AI, Razi H, Duda GN, Checa S, Willie BM. 2017 Tomography-based quantification of regional differences in cortical bone surface remodeling and mechano-response. *Calcif. Tissue Int.* **100**, 255–270. (doi:10.1007/s00223-016-0217-4)
22. Holguin N, Brodt MD, Silva MJ. 2016 Activation of wnt signaling by mechanical loading is impaired in the bone of old mice. *J. Bone Miner. Res.* **31**, 2215–2226. (doi:10.1002/jbmr.2900)
23. Cosman F *et al.* 2016 Romosozumab treatment in postmenopausal women with osteoporosis. *N. Engl. J. Med.* **375**, 1532–1543. (doi:10.1056/NEJMoa1607948)
24. McClung MR *et al.* 2014 Romosozumab in postmenopausal women with low bone mineral density. *N. Engl. J. Med.* **370**, 412–420. (doi:10.1056/NEJMoa1305224)
25. Glorieux FH *et al.* 2017 BPS804 anti-sclerostin antibody in adults with moderate osteogenesis imperfecta: results of a randomized phase 2a trial. *J. Bone Miner. Res.* **32**, 1496–1504. (doi:10.1002/jbmr.3143)
26. Doube M, Kłosowski MM, Arganda-Carreras I, Cordeliéres F, Dougherty RP, Jackson J, Schmid B, Hutchinson JR, Shefelbine SJ. 2010 BoneJ: free and extensible bone image analysis in ImageJ. *Bone* **47**, 1076–1079. (doi:10.1016/j.bone.2010.08.023)
27. Willie BM *et al.* 2013 Diminished response to *in vivo* mechanical loading in trabecular and not cortical bone in adulthood of female C57Bl/6 mice coincides with a reduction in deformation to load. *Bone* **55**, 335–346. (doi:10.1016/j.bone.2013.04.023)
28. Razi H *et al.* 2015 Skeletal maturity leads to a reduction in the strain magnitudes induced within the bone: a murine tibia study. *ActaBiomaterialia* **13**, 301–310. (doi:10.1016/j.actbio.2014.11.021)

29. Yang H *et al.* 2017 Examining tissue composition, whole-bone morphology and mechanical behavior of Gorab(Prx1) mice tibiae: a mouse model of premature aging. *J. Biomech.* **65**, 145–153. (doi:10.1016/j.jbiomech.2017.10.018)
30. Cao L, Youn I, Guilak F, Setton LA. 2006 Compressive properties of mouse articular cartilage determined in a novel micro-indentation test method and biphasic finite element model. *J. Biomech. Eng.* **128**, 766–771. (doi:10.1115/1.2246237)
31. Yang H, Butz KD, Duffy D, Niebur GL, Nauman EA, Main RP. 2014 Characterization of cancellous and cortical bone strain in the *in vivo* mouse tibial loading model using microCT-based finite element analysis. *Bone* **66**, 131–139. (doi:10.1016/j.bone.2014.05.019)
32. Zou W, Hunter N, Swain MV. 2011 Application of polychromatic μCT for mineral density determination. *J. Dent. Res.* **90**, 18–30. (doi:10.1177/0022034510378429)
33. Birkhold AI, Razi H, Duda GN, Weinkamer R, Checa S, Willie BM. 2016 The periosteal bone surface is less mechano-responsive than the endocortical. *Sci. Rep.* **6**, 23480. (doi:10.1038/srep23480)